Geophysical Journal International

Geophys. J. Int. (2016) **204,** 1789–1800 doi: 10.1093/gji/ggv552

GJI Geomagnetism, rock magnetism and palaeomagnetism

Evidence for MAC waves at the top of Earth's core and implications for variations in length of day

Bruce Buffett,[1] Nicholas Knezek[1] and Richard Holme[2]

[1] *Department of Earth and Planetary Sciences, University of California, Berkeley, CA* 94720*, USA. E-mail: bbuffett@berkeley.edu*

[2] *School of Environmental Sciences, University of Liverpool, Liverpool* L69 3GP*, United Kingdom*

Accepted 2015 December 23. Received 2015 December 23; in original form 2015 September 28

SUMMARY

Earth's liquid core hosts a diverse set of waves with periods ranging from days to thousands of years. One class of waves with periods of several decades is known to arise from an interplay between magnetic, Archimedes and Coriolis forces. These so-called MAC waves are thought to be relevant for interpreting historical fluctuations in the geomagnetic field. In this study, we show that MAC waves provide a good description of time-dependent zonal flow at the top of the core. The same collection of waves also offers a simple explanation for observed fluctuations in the dipole field. Both of these predictions require a stratified layer at the top of the core with a thickness of 130–140 km and a buoyancy frequency comparable to Earth's rotation rate. We extend these predictions to include changes in the length of day (LOD) and find that MAC waves can account for about half of the observed fluctuation at decadal periods. Larger fluctuations are possible when electromagnetic stresses couple MAC waves to flow in the interior of the core. In fact, an idealized model for the coupled motion overestimates the LOD fluctuations, probably reflecting limitations in this idealized model. Our results offer support for stable stratification at the top of the core and suggest a common origin for decadal fluctuations in the geomagnetic field and the LOD.

Key words: Earth rotation variations; Geomagnetic induction; Rapid time variations.

1 INTRODUCTION

Waves in Earth's core are often invoked to explain fluctuations in the geomagnetic field with periods of several decades (Hide 1966). Initial attempts to identify these waves appealed to a class of magnetic waves, known as torsional oscillations (Braginsky 1970), which represent a transient response to disturbances in the primary force balance in the core (Jones 2011). The associated flow is organized into the form of cylinders that align with the rotation axis due to the strong influence of planetary rotation. Motion between adjacent cylinders distorts any magnetic field that crosses the cylinder surfaces, providing the necessary restoring force for wave motion (Jault & Finlay 2015). Waves with periods of several decades imply a relatively weak magnetic field (Zatman & Bloxham 1997; Buffett *et al.* 2009), whereas numerical geodynamo models predict a much stronger internal magnetic field (Christensen 2011). More recent interpretations of core-surface flow now favour torsional waves with periods of 4–6 yr (Gillet *et al.* 2010), providing better agreement with numerical geodynamo models (Teed *et al.* 2014). However, this consensus leaves the origin of longer period fluctuations unknown.

Waves with periods of several decades can arise when the top of the liquid core is stably stratified (Braginsky 1993). A balance between buoyancy, rotation and magnetic forces (sometimes called a MAC balance) permits long-period motion with almost no influence from inertia. Instead, slow radial motion alters the pressure field in the presence of a background stratification (see Fig. 1). Horizontal pressure gradients sustain a geostrophic flow, which continually adjusts to the changing radial position of buoyant parcels. This geostrophic flow distorts the radial magnetic field, inducing a weaker poleward flow. The feedback of this poleward flow on the radial motion closes the chain of interactions that permit the so-called MAC waves. Nominal wave periods are set by the strength of the fluid stratification and by the amplitude of the radial magnetic field. The thickness of the layer has a principal role in determining the damping of the waves.

Braginsky (1993) showed that MAC waves with periods of 30–60 yr could be realized with plausible values for the fluid stratification and radial magnetic field. He was able to obtain analytical solutions for the waves when the radial magnetic field was restricted to the form of a dipole. However, detailed tests of these waves with available observations suggest that a more general description of the radial magnetic field is required if we want to link core-surface flows to fluctuations in the dipole field (Buffett 2014). The difficulty arises because the shapes of waves in the presence of a dipole field are not compatible with both the core-surface flow and the dipole fluctuations. Both phenomena can be reconciled by modifying the spatial structure of the modes through a change in the spatial distribution of the radial magnetic field over the core–mantle boundary.

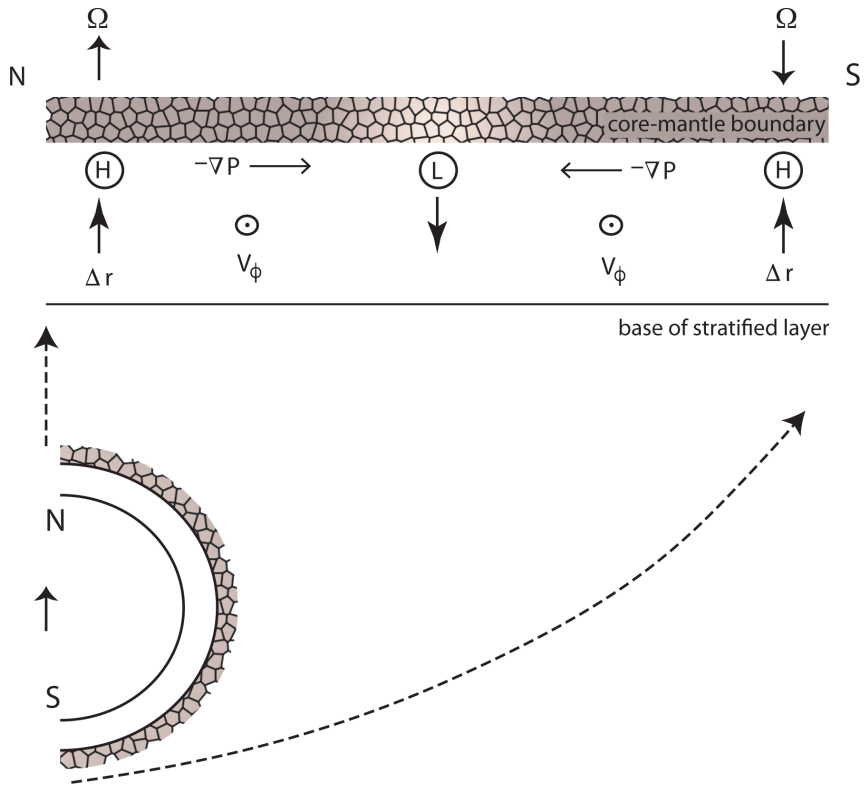

Figure 1. Schematic illustration of a MAC wave at the top of the core. A radial displacement, Δr, disturbs the density distribution, creating regions of high (H) and low (L) pressure. The influence of rotation, $\mathbf{\Omega}$, promotes a balance between the horizontal pressure gradient and a geostrophic flow $\mathbf{v}_\phi$ (directed out of the page). Tension in the radial magnetic field opposes $\mathbf{v}_\phi$, inducing a meridional flow toward the north (N) and south (S) poles.

A simple, but plausible alternative is to assume that the radial field is randomly distributed over the surface of the core with nearly equal power across a broad range of spatial scales. Because the magnetic restoring force does not depend on the direction of the radial field, a uniform spectrum can be approximated as a constant root-mean-squared (rms) radial field, at least for the purposes of predicting the waves. Good agreement with available estimates for core-surface flows and dipole fluctuations requires a stratified layer with a buoyancy frequency comparable to the Earth's rotation rate (Buffett 2014).

Geodetic observations of fluctuations in the length of day (LOD) are also known to exhibit fluctuations with periods of several decades (Gross 2001; Holme & de Viron 2005). These fluctuations are commonly attributed to exchanges of angular momentum between the core and the mantle. Similarities between the LOD and geomagnetic fluctuations have prompted speculations about a common origin (Braginsky 1984). While torsional waves can account for the LOD fluctuations (Braginsky 1970), a purely toroidal flow does not contribute to variations in the dipole field. Here we assess whether MAC waves offer a viable interpretation for both phenomena.

A primary focus in this study is to quantify the role of MAC waves on LOD fluctuations. We find that MAC waves in a layer at the top of the core carry angular momentum, which permits a change in LOD. By fitting a linear combination of waves to the core-surface flow of Jackson (1997), we can account for roughly half of the observed, long-period change in LOD solely from motions within this layer. The other half could arise from the influence of electromagnetic stresses exerted by the waves on the interior of the core. We predict torques on the order of 10^{18} N m, which are large enough to explain the typical amplitude of LOD variations. In some instances, the predicted torques can actually be too large. One interpretation of the excessive LOD predictions is that the interior flow has an important feedback on the MAC waves. In this case, an isolated treatment of MAC waves may not be sufficient to fully describe the dynamics.

Extensions of the MAC-wave model to include the response of the interior of the core have a chain of consequences. Motion of the interior due to electromagnetic stresses would tend to reduce differential motion between the stratified layer and interior. The corresponding reduction in electromagnetic stresses would lower the torque, potentially yielding better agreement with the LOD observations. While a fully coupled treatment of the dynamics of the interior is beyond the scope of the current work, we do consider one idealized case to illustrate a few basic features of the coupled problem.

Another motivation for the present work is to correct a minor error in the wave calculations in Buffett (2014). As shown below, the error has only a small effect on the structure of the waves, so the previous conclusions are not changed. However, some of the specific predictions for the wave periods and damping are revised.

2 DESCRIPTION OF MAC WAVES

MAC waves can be represented as small perturbations in velocity, $\mathbf{v}$, and magnetic field, $\mathbf{b}$. We assume that these perturbations are superimposed on background fields, $\mathbf{V}$ and $\mathbf{B}$, which are taken to be steady over the period of the waves. The shallow depth of the layer means that radial gradients in the perturbations are much larger than horizontal gradients. Terms like $\mathbf{B} \cdot \nabla \mathbf{v}$ in the induction

equation can be approximated by $B_r\partial_r\mathbf{v}$, indicating that the radial magnetic field, B_r, has a primary role in the dynamics. Following Braginsky (1993) we let $\mathbf{V} = 0$ and retain only the radial part of $\mathbf{B}$. With these approximations the linearized equations for $\mathbf{v}$ and $\mathbf{b}$ are

$$\rho(\partial_t\mathbf{v} + 2\boldsymbol{\Omega}\times\mathbf{v}) = -\nabla P + \frac{1}{\mu}B_r\partial_r\mathbf{b} + \Delta\rho\mathbf{g} + \rho\nu\nabla^2\mathbf{v} \tag{1}$$

$$\partial_t\mathbf{b} = B_r\partial_r\mathbf{v} + \eta\nabla^2\mathbf{b} \tag{2}$$

$$\nabla\cdot\mathbf{v} = \nabla\cdot\mathbf{b} = 0 \tag{3}$$

where ρ is the fluid density, $\boldsymbol{\Omega} = \Omega\hat{\mathbf{z}}$ is the mean rotation rate of the Earth, μ is the magnetic permeability, $\Delta\rho$ is the density perturbation, $\mathbf{g} = -g\hat{\mathbf{r}}$ is the acceleration due to gravity, ν is the fluid viscosity and $\eta = (\mu\sigma)^{-1}$ is the magnetic diffusivity. Here σ is the electrical conductivity of the core.

Density perturbations in the Boussinesq approximation arise from radial motion through a background stratification. This stratification may be due to temperature or composition, but its origin is not important as long as the effects of thermal or compositional diffusion are small over one cycle. Under this approximation, the density perturbation can be written as

$$\Delta\rho = -\mathbf{u}\cdot\nabla\rho \approx -u_r\frac{\partial\rho}{\partial r} \tag{4}$$

where $\mathbf{u}$ is the displacement associated with the wave. For small-amplitude waves

$$\partial_t\mathbf{u} = \mathbf{v}\,. \tag{5}$$

Radial variations in density due to hydrostatic pressure do not contribute to the buoyancy force, so the radial derivative in (4) is defined relative to variations in a well-mixed, isentropic fluid. It is convenient to express the density gradient in terms of a buoyancy frequency

$$N = \sqrt{-\frac{g}{\rho}\frac{\partial\rho}{\partial r}} \tag{6}$$

which defines the hypothetical frequency of a fluid parcel oscillating in a density stratification without the effects of rotation and a magnetic field.

The governing equations are written in non-dimensional form using the radius of the core, R, as the lengthscale, Ω^{-1} as the timescale and $\sqrt{\Omega\rho\mu\eta}$ as the scale for the magnetic field. The resulting dimensionless equations are

$$\partial_t\mathbf{v} + 2\hat{\mathbf{z}}\times\mathbf{v} = -\nabla P + E_\eta B_r\partial_r\mathbf{b} - \tilde{N}^2(\mathbf{u}\cdot\hat{\mathbf{r}})\hat{\mathbf{r}} + E\nabla^2\mathbf{v} \tag{7}$$

$$\partial_t\mathbf{b} = B_r\partial_r\mathbf{v} + E_\eta\nabla^2\mathbf{b} \tag{8}$$

where the dimensionless parameters

$$\tilde{N}^2 = \frac{N^2}{\Omega^2}, \quad E = \frac{\nu}{\Omega R^2}, \quad E_\eta = \frac{\eta}{\Omega R^2} \tag{9}$$

are, respectively, a (squared) dimensionless buoyancy frequency, the Ekman number and a parameter sometimes called the magnetic Ekman number (Christensen *et al.* 2010). The model used here is similar to one used by Braginsky (1993), but we retain the effects of local inertia in (7) and include all components of the rotation vector in the Coriolis force. We also retain the viscous force, whereas Braginsky (1993) assumes inviscid flow.

2.1 Boundary conditions

Solutions to (7) and (8) are subject to boundary conditions at the top and bottom of the stratified layer. Viscous stress-free conditions are imposed on the top and bottom boundaries to eliminate viscous boundary layers, thus reducing the demands on numerical resolution. No radial motion is permitted at the core–mantle boundary, under the assumption that the deformation of the mantle is small. Below the stratified layer we expect fluid motion to take the form of torsional oscillations (Braginsky 1970). The quasi-geostrophic nature of this motion ensures that the radial component of flow is small. Consequently, we impose no radial motion at the base of the layer. While buoyant fluid parcels below the layer can induce radial motion, we treat this motion as part of the excitation source rather than as part of the wave. Indeed, numerical calculations in Buffett (2014) confirm that radial motion in the bulk of the neutrally stratified interior is small. This condition prevails at the base of the stratified layer, where the strength of stratification vanishes (see below).

The magnetic field at the top of the layer is continuous with a potential field outside the core under the approximation that the mantle is an electrical insulator. A more general electromagnetic condition is needed at the base of the layer because viscous stress-free conditions on velocity permit discontinuities in the horizontal velocity. A suitable condition is obtained by combining the requirements of continuity of the magnetic field and continuity of the horizontal electric field (Gubbins & Roberts 1987). The condition on the electric field can be written in spherical coordinates (r, θ, ϕ) as

$$[\eta\,\partial_r b_{\theta,\phi}]^+_- + B_r[v_{\theta,\phi}]^+_- = 0 \tag{10}$$

where $[\,]^+_-$ denotes the jump in the enclosed quantity across the base of the layer. To be specific in our discussion we let subscript $-$ indicate the lower (interior) side of the interface and superscript $+$ represent the upper (layer) side of the interface.

The continuity condition in (10) requires a solution for the magnetic perturbation in the interior of the core. A simple solution is obtained when the wave motion is confined to the stratified layer and the flow in the underlying region vanishes (i.e. $\mathbf{v}^- = 0$). In this case, the magnetic perturbation obeys a diffusion equation in the interior of the core. Solutions with time dependence of the form $e^{i\omega t}$ can be approximated by

$$b^-_{\theta,\phi}(r,\theta,\phi) = b^-_{\theta,\phi}(r_i,\theta,\phi)\,e^{(1+i)(r-r_i)/\delta} \tag{11}$$

where

$$\delta = \sqrt{\frac{2\eta}{\omega}} \tag{12}$$

is the skin depth and r_i is the radius of the interface between the layer and the interior of the core. This particular approximation depends on δ being small compared with the lengthscale for horizontal variations. An identical solution for $\mathbf{b}^-$ would also be appropriate when the interior velocity is characterized by a large-scale geostrophic flow because the horizontal lengthscales are large compared with the skin depth. In either case the induced magnetic perturbation in the interior is due mainly to a velocity discontinuity at r_i. Thus, the interior solution represents a diffusive perturbation near the boundary.

Invoking the continuity of magnetic field in (10) yields

$$\partial_r b^+_{\theta,\phi} - (1+i)\,\frac{b^+_{\theta,\phi}}{\delta} + \frac{B_r}{\eta}(v^+_{\theta,\phi} - v^-_{\theta,\phi}) = 0 \tag{13}$$

where η is assumed to be continuous inside the core. Setting $\mathbf{v}^- = 0$ defines a homogeneous boundary condition at the bottom of the

stratified layer, which fully specifies the solution for $\mathbf{b}^+$ when combined with the insulating condition at the top. Restoring the interior flow to the wave problem requires a separate description of the dynamics in the interior. Several possibilities are discussed below, but most of the subsequent results are obtained using $\mathbf{v}^- = 0$. Another complication arises with the frequency dependence of the skin depth in (12). Numerical solutions for the waves can be obtained using standard methods once a rough estimate is given for the skin depth. The resulting solution for the eigenfrequency can then be used to update the skin depth and the calculation is repeated. Corrections to the eigenfrequencies are typically very small, so one iteration is usually sufficient to obtain accurate solutions.

2.2 Numerical solution

Solenoidal conditions on $\mathbf{v}$ and $\mathbf{b}$ in (3) are imposed using a toriodal–poloidal decomposition (Kuang & Bloxham 1999). The toroidal and poloidal scalars are expanded in fully normalized spherical harmonics with coefficients that depend on radius, r, and time, t. Each coefficient corresponds to a particular degree, l, and order, m, in the spherical harmonic expansion. The time dependence for all coefficients (say v_l^m) is represented in the form

$$v_l^m(r,t) = \tilde{v}_l^m(r) e^{i\omega t} \tag{14}$$

where ω is the frequency of the wave. Radial derivatives in the governing equations are approximated by second-order finite differences on an evenly spaced grid in radius.

Substituting the spherical harmonic expansions into the governing equations defines a system of algebraic equations of the form

$$A\mathrm{x} = \omega B\mathrm{x} \tag{15}$$

where x is a vector of scalar coefficients for $\mathbf{v}$, $\mathbf{b}$ and $\mathbf{u}$ at the radial gridpoints. Similarly, the boundary conditions can be written in matrix form as

$$C\mathrm{x} = 0 \tag{16}$$

The governing equations and boundary conditions can be combined into a single matrix equation

$$\begin{bmatrix} A & C^T \\ C & 0 \end{bmatrix} \begin{bmatrix} \mathbf{x} \\ \epsilon \end{bmatrix} = \omega \begin{bmatrix} B & 0 \\ 0 & 0 \end{bmatrix} \begin{bmatrix} \mathbf{x} \\ \epsilon \end{bmatrix} \tag{17}$$

where the auxiliary variables, ϵ, tend to decrease in amplitude as the resolution of the numerical solution improves (Fox & Parker 1968). Iterative solutions for the complex eigenvalues, ω, are obtained using an implicitly restarted Arnoldi method (Lehoucq & Sorensen 1996).

Numerical solutions are obtained on a radial grid with 200 radial levels, and the spherical harmonic expansion is truncated at $l = 40$. Solutions for zonal waves ($m = 0$) fall into two classes, depending on whether the radial flow is symmetric or antisymmetric about the equator. We confine our attention to symmetric waves because the associated azimuthal flow, $\mathbf{v}_\phi$, is directly comparable to the zonal flows inferred from geomagnetic secular variation (Jackson 1997; Gillet *et al.* 2015).

3 REPRESENTATIVE SOLUTION FOR MAC WAVES

Our numerical calculations are specified by the three dimensionless parameters in (9) and by the strength of the radial magnetic field. Indirect inferences of B_r from geodetic observations (Buffett *et al.* 2002; Koot *et al.* 2010), as well as numerical geodynamo models (Christensen 2011), suggest that a large part of the radial magnetic field resides in wavelengths that are too small to detect at the Earth's surface. We adopt a simple description by assuming that the radial magnetic field is randomly distributed over the core–mantle boundary. Because the waves do not depend on the direction of the magnetic field, the rms value can be approximated as a constant in the calculations. Here we take $B_r = 0.62$ mT, which is sufficient to explain the geodetic observations when the electrical conductivity is $\sigma = 10^6$ S m^{-1} (Pozzo *et al.* 2012). Combining this value for σ with the permeability of free space, $\mu = 4\pi \times 10^{-7}$ H m^{-1}, gives a magnetic diffusivity of $\eta = 0.8$ m^2 s^{-1}. Standard values for $R = 3.48 \times 10^6$ m, $\Omega = 0.729 \times 10^{-4}$ s^{-1} and $\rho = 10^4$ give a characteristic magnetic field of $\sqrt{\Omega\rho\mu\eta} = 0.86$ mT and a magnetic Ekman number of $E_\eta = 9 \times 10^{-10}$. Finally, we adopt a turbulent value for $\nu \approx \eta$, which gives $E = E_\eta$, although the resulting waves are relatively insensitive to the choice of E when stress-free boundary conditions are imposed.

The properties of the stratified layer are specified by its thickness, H, and by the buoyancy frequency, N. For simplicity H is assumed to be constant and N is allowed to vary linearly with radius across the layer, broadly consistent with expectations for thermal stratification (Lister & Buffett 1998). The value of N is largest at the core–mantle boundary and decreases to zero at the base of the stratified. As a result, the structure of the layer is completely determined by H and the maximum value of N (denoted as $N_{\max}$). Both H and $N_{\max}$ are subsequently treated as adjustable parameters when we seek to interpret core-surface flow in terms of MAC waves (see Section 4). Here we adopt plausible values ($H = 140$ km and $N_{\max} = 0.84\,\Omega$) to calculate the real and imaginary parts of a typical wave. The wave shown in Figs 2 and 3 has a symmetric pattern of radial flow, $\mathbf{v}_r$, which is roughly described by a zonal spherical harmonic with degree $l = 4$. In detail the waves are more complicated than a single spherical harmonic degree, but the dominant pattern is useful for characterizing the different waves. The gravest waves have upwellings at the poles and a downwelling at the equator over half of a cycle (corresponding to $l = 2$). Overtones have more complicated structure in radius and are more heavily damped than the fundamental modes. Waves with a larger number of upwellings and downwellings (i.e. larger l) have shorter periods.

Symmetries in the radial motion in Figs 2 and 3 are mirrored in the azimuthal flow, $\mathbf{v}_\phi$, which is driven by pressure perturbations associated with $\mathbf{v}_r$. A weaker meridional flow, $\mathbf{v}_\theta$, is induced by the effects of magnetic friction on the azimuthal flow. The peak azimuthal flow occurs slightly below the core–mantle boundary in Fig. 2. As time advances by half a cycle (Fig. 3), the peak azimuthal flow shifts toward the core–mantle boundary. One implication of this result is that the angular momentum of a wave cannot be directly assessed from flow at the core–mantle boundary. Another point to note is that the large azimuthal flow is nearly geostrophic. Lorentz forces induce a meridional flow, but the amplitude of this flow is about an order of magnitude smaller than $\mathbf{v}_\phi$. Thus, the departures from tangential geostrophy are about 10 per cent in this particular example.

Table 1 lists the periods and quality factors for two sets of waves. One set of waves is defined by fitting the core-surface flow of Jackson (1997), which is based on the geomagnetic field model GUFM1 (Jackson *et al.* 2000). The other set of waves is obtained by fitting the flow model of Gillet *et al.* (2015), based on the geomagnetic field model COV-OBS (Gillet *et al.* 2013). The period and quality factors listed under GUFM1 were calculated with a layer thickness $H = 140$ km and a stratification $N_{\max} = 0.84\,\Omega$, whereas

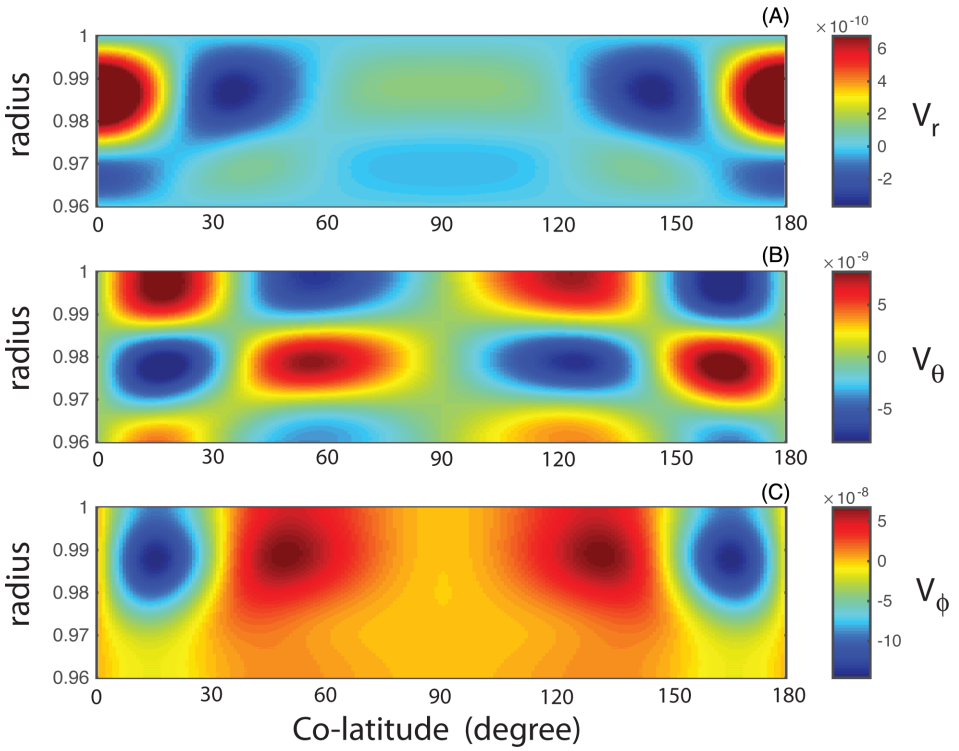

Figure 2. The real part of the velocity field for a typical MAC. The flow has components in the (A) radial, (B) meridional and (C) azimuthal directions. This particular wave is specified by $l = 4$ and $n = 0$, corresponding to the dominant spherical harmonic degree l of radial velocity and the radial overtone n. The radial velocity, $\mathbf{v}_r$, induces a large geostrophic flow, $\mathbf{v}_\phi$, with a peak velocity below the core–mantle boundary. The meridional flow, $\mathbf{v}_\theta$ is about an order of magnitude smaller than $\mathbf{v}_\phi$.

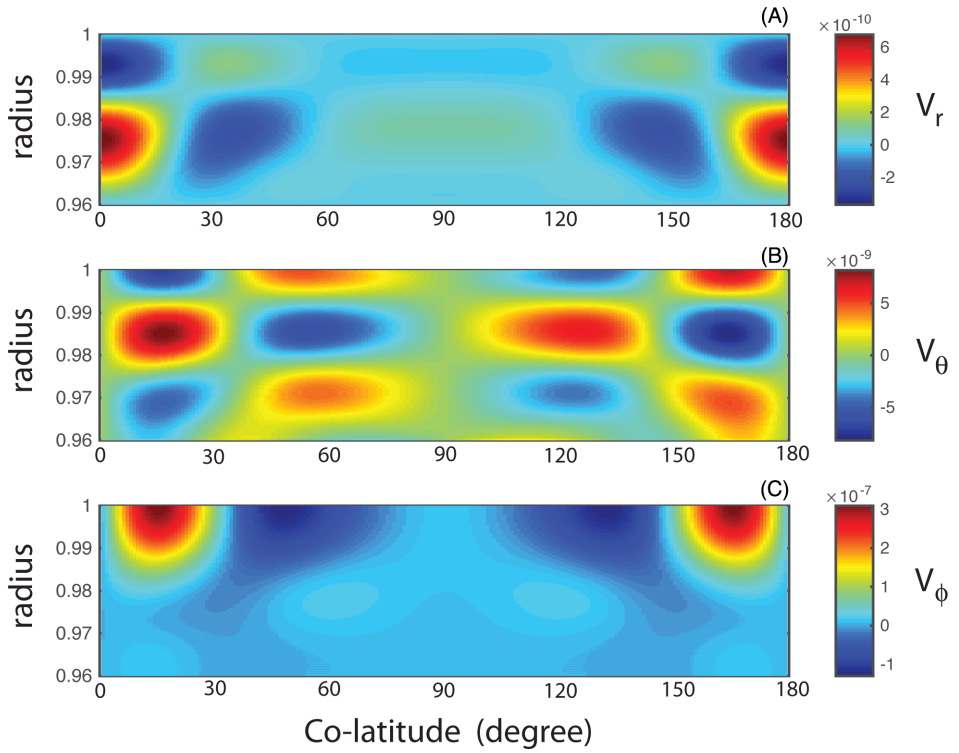

Figure 3. The imaginary part of the velocity field for a typical MAC ($l = 4$, $n = 0$). The relative magnitudes of the (A) radial (B) meridional and (C) azimuthal components of flow are comparable to those in the real part of the velocity field, although the radial structure is somewhat different. The largest radial flow occurs deeper in the layer and the peak azimuthal flow occurs at the core–mantle boundary.

Table 1. MAC wave period, P, qualify factor, Q and fit to surface core flow.

Mode	Overtone	GUFM1			COV-OBS		
l	n	P (yr)	Q	Fit (per cent)	P (yr)	Q	Fit (per cent)
2	0	116.47	2.47	1.3	133.13	2.24	0.9
2	1	134.86	0.85	0.0	175.13	0.51	0.0
4	0	57.40	2.77	29.1	68.07	2.42	28.8
4	1	71.35	1.71	9.6	77.98	1.39	19.2
6	0	37.82	3.17	7.7	43.93	2.76	8.0
6	1	51.19	1.75	29.8	55.68	1.78	22.9
8	0	28.04	3.73	5.0	32.38	3.00	4.6
8	1	41.35	1.78	16.2	43.85	1.81	15.6

the waves listed under COV-OBS were calculated with $H = 129$ km and $N_{\max} = 0.74\,\Omega$. Details of the fitting procedure are given in Section 4. Here it suffices to note that the waves are classified according to the dominant spherical harmonic degree of the radial wave motion. We also distinguish between the fundamental mode ($n = 0$) and the first overtone ($n = 1$). Higher overtones ($n > 1$) are heavily damped, making them less likely to detect in surface observations. The quality factor is approximated by

$$Q = \frac{Re(\omega)}{2Im(\omega)}. \tag{18}$$

One surprising feature of the waves is that the first overtone has a longer period than the fundamental mode. This behaviour is attributed to the fact that overtones have larger radial motion near the bottom of the stratified layer, where the strength of the stratification is weaker. A weaker restoring force lengthens the period of the overtones. By comparison, waves in a layer with constant stratification (not shown) have nearly identical periods for the fundamental and first overtone. The quality factors for waves with constant N are similar to the values shown in Table 1.

4 INTERPRETATION OF CORE-SURFACE FLOW

Estimates of time-dependent flow at the top of the core offer a quantitative assessment of MAC waves. We focus initially on the flow model of Jackson (1997), although we also consider a second flow model from Gillet *et al.* (2015) to assess the consistency of our interpretation. The model of Jackson (1997) relies on tangential geostrophy as a constraint to reduce non-uniqueness in the inversion (e.g. Holme 2015). Strictly enforcing tangential geostrophy means that the zonal flow is purely toroidal. The symmetric part of this flow contains most of the time dependence, so we limit our attention to flow with odd spherical harmonic degrees. We also confine our analysis to the largest spatial scales to reduce the unwanted influence of unresolved features in the geomagnetic field and flow (Eymin & Hulot 2005). In our subsequent discussion, we retain only the spherical harmonic components of flow with degrees $l = 1$, 3 and 5.

The symmetric part of $\mathbf{v}_\phi$ from the tangentially geostrophic flow of Jackson (1997) is shown in Fig. 4. The results are displayed as a function of $\sin\theta$, where θ is colatitude, because the motion in the Northern and Southern Hemispheres is the same. In addition, we confine the record to a 60-yr interval between 1930 and 1990. This interval is long enough to capture the decadal fluctuations, but short enough to consider the role of waves with constant amplitude and phase.

The question posed here is whether $\mathbf{v}_\phi$ can be described by MAC waves. We treat the layer thickness, H, and the peak stratification, $N_{\max}$ as adjustable parameters in the wave calculation and fit a linear combination of the eight gravest modes to the flows of Jackson (1997). All of the predicted waves are filtered to remove $l > 5$, consistent with the flow model. Iterative adjustments to H and $N_{\max}$ are used to minimize the misfit, yielding the predictions shown in Fig. 4(B). The best-fitting results are achieved with $H = 140$ km and $N_{\max} = 0.84\,\Omega$. These values differ slightly from those reported previously in Buffett (2014). A minor error in the previous calculations had the effect of reducing the strength of the radial main field, requiring a larger stratification ($N^2_{\max} = 1.02\,\Omega^2$ or $N_{\max} = 1.01\,\Omega$) to match $\mathbf{v}_\phi$. Correcting the error lowered the strength of the stratification, but this change had little effect on the spatial structure of the waves.

Good agreement between the flow model and the prediction of the MAC waves means that the flow can be adequately represented by a small number of MAC waves. The input flow model is described by three spherical harmonic coefficients ($l = 1$, 3 and 5) at 15 epochs for a total of 45 data points, whereas the wave prediction relies on 8 (complex) amplitudes once the values of H and $N_{\max}$ are prescribed. Over two-thirds of the flow is attributed to only four waves (with dominant radial motion at $l = 4$ and 6), which means that reasonable fits could be achieved with a smaller set of waves. While these fits are encouraging, it is quite likely that a linear combination of waves could be adapted to explain the periodic nature of flow in the model of Jackson (1997).

A second model for core-surface flow due to Gillet *et al.* (2015) permits another test using more recent magnetic-field observations. An ensemble of flows were constructed by treating the unresolved magnetic field and core-surface motion as stochastic processes. Flows over the time interval 1940–2010 were constrained using the condition of quasi-geostrophy (Amit & Olson 2004) and the assumption of equatorial symmetry (Pais & Jault 2008). Thus, we focus exclusively on the symmetric waves, as was done previously with the flow model of Jackson (1997). A preference for symmetric waves might be attributed to the nature of the excitation mechanism. A focusing of upwelling into the equatorial region, as seen in some geodynamo models (e.g. Matsui *et al.* 2014), could account for the generation of symmetric waves. We fit a set of symmetric waves to the ensemble average over a 60-yr interval (1950–2010), after removing the time average. Iteratively adjusting the layer properties yields a best fit at $H = 129$ km and $N = 0.74\,\Omega$. A slightly lower buoyancy frequency means that the wave periods are somewhat longer than those inferred from GUFM1 (see Table 1). The longest period wave (now $P = 175$ yr for the $l = 2$ and $n = 1$ mode) was too long to reliably fit to flow to a 60-yr interval, so we exclude this wave from the fit. For the sake of consistency, we exclude the same wave from the fits to the flow based on GUFM1, although the differences are small.

Both flow models yield similar results for the properties of the stratified layer. The resulting wave periods from COV-OBS are slightly longer than those inferred from GUFM1, whereas the

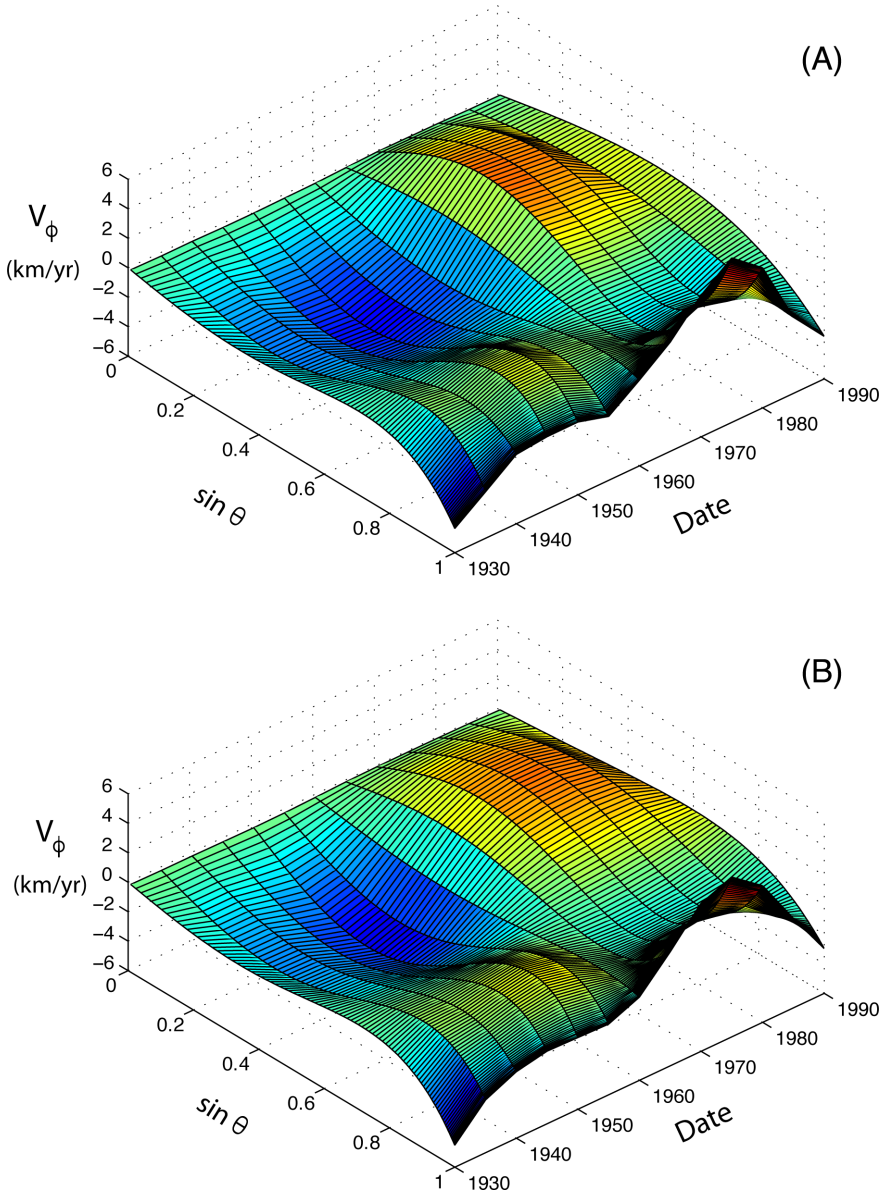

Figure 4. (A) Low-degree part of the zonal flow from the model of Jackson (1997) as a function of $\sin\theta$ and time t. (B) A prediction for the best-fitting linear combination of MAC waves, calculated using $H = 140$ km and $N_{\max} = 0.84\,\Omega$.

quality factors are generally lower. On the other hand, the relative contributions of the various waves to the core-surface flow are broadly similar between the two flow models. The majority of the flow for both GUFM1 and COV-OBS can explained by the same four waves. Even the relative amplitudes of those waves are comparable (see Table 1). We conclude that MAC waves are compatible with the flow, but a more extensive test is possible using predictions for the dipole fluctuations and the associated changes in LOD. A key point to note below is that there are no adjustable parameters once the waves have been fit to estimates of $\mathbf{v}_\phi$.

5 FLUCTUATIONS IN DIPOLE FIELD

A large part of each wave is comprised of a nearly geostrophic flow $\mathbf{v}_\phi$. A weaker meridional flow, $\mathbf{v}_\theta$, is induced by the effects of magnetic friction on $\mathbf{v}_\phi$. Once a linear combination of waves are fit to an estimate of $\mathbf{v}_\phi$, the associated meridional flow sweeps the radial magnetic field toward the pole. The resulting fluctuations in the radial magnetic field, b_r, are described by

$$\partial_t b_r = -\nabla_H \cdot (\mathbf{v} B_r) + \frac{\eta}{r}\nabla^2 (r b_r) \tag{19}$$

where $\nabla_H \cdot$ denotes the horizontal part of the divergence operator. Recall that B_r is the steady background radial field and b_r is the perturbation associated with the waves. Thus, the horizontal divergence in (19) represents the influence of wave velocity, $\mathbf{v}$, on the steady main field. The magnetic fluctuation is also affected by magnetic diffusion, which arises primarily from radial gradients in b_r. We approximate the diffusive term using a characteristic radial lengthscale, H/π, and write the induction equation for b_r in the form

$$\left(\partial_t + \eta \frac{\pi^2}{H^2}\right) b_r = -\nabla_H \cdot (\mathbf{v} B_r) \tag{20}$$

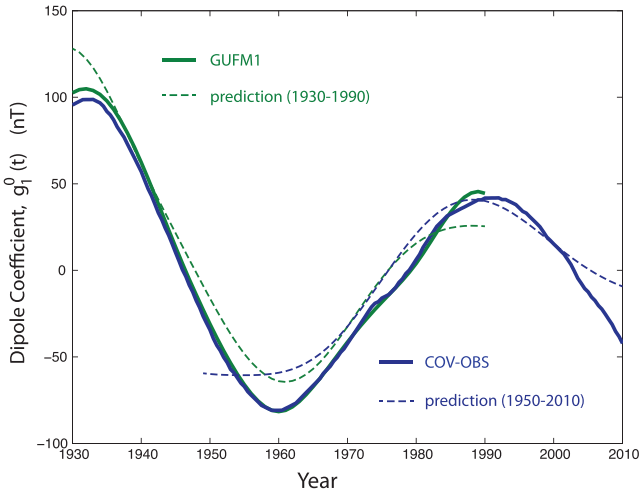

Figure 5. Fluctuations in the dipole field are computed from geomagnetic field models GUFM1 (Jackson *et al.* 2000) and COV-OBS (Gillet *et al.* 2013), after removing a linear trend. The predicted dipole fluctuations (dashed lines) are based on fitting a linear combination of MAC waves to the core-surface flow over the intervals 1930–1990 and 1950–2010.

which is solved numerically for each wave using the method of finite differences in spherical coordinates. The total magnetic fluctuation is predicted using the linear combination of waves that fit $\mathbf{v}_\phi$.

It is important to distinguish between the role of B_r in the wave dynamics and its contribution to the dipole fluctuation in (20). All spherical harmonic components of B_r influence the spatial structure of the waves through the effects of magnetic friction. We have previously assumed that B_r is randomly distributed over a large number of spherical harmonics. Because magnetic friction does not depend on the sign of B_r we can reasonably approximate B_r^2 as a constant over the core–mantle boundary. However, we do not expect the short-wavelength components of B_r to contribute much to the magnetic fluctuations at Earth's surface. The MAC waves considered in this study are predominantly long wavelength, so a short-wavelength component of B_r will induce a short-wavelength component of b_r at the core–mantle boundary. We have no hope of detecting this short-wavelength perturbation at the surface, even though this short-wavelength perturbation has an important influence on the dynamics. Only odd zonal spherical harmonics in B_r contribute to b_r because of the symmetry of the waves, and we can safely focus on the longest wavelength components to compute b_r at the surface. The largest contribution to b_r comes from the dipole part of B_r, but we retain all odd zonal components from the GUFM1 field model (Jackson *et al.* 2000) for the mid-range epoch of 1960. Similarly, we use the odd zonal components from the COV-OBS field model (Gillet *et al.* 2013) at 1980 when computing dipole fluctuations from the waves based on the flow model of Gillet *et al.* (2015). The dipole component of b_r is recovered from the numerical solution using the orthogonality of spherical harmonics.

Fig. 5 compares the predicted dipole fluctuation with the time variations in the GUFM1 and COV-OBS models, after removing a linear trend. The amplitude and phase of the dipole fluctuation agree reasonably well with the predictions based on MAC waves. Even the gradual decay of the dipole fluctuation is captured by the waves, although the predicted decay appears to be more rapid than the observations. Better agreement with the dipole fluctuations (but not the core flow) might be achieved by reducing the damping of the waves. One way to reduce the damping is to increase the thickness of the layer. Unfortunately, this change has the unwanted consequence of decreasing the amplitude of the dipole fluctuation (see Appendix A). Alternatively, we could lower the wave damping by changing boundary conditions at the base of the layer. A large part of the damping is associated with electromagnetic stresses at the base of the layer. These stresses suppress horizontal motion at the base of the layer when the interior is stationary. Less damping is expected when the interior is allowed to move in response to electromagnetic stresses. A smaller velocity discontinuity at the base of the layer would reduce the electric currents and lower damping. Thus accounting for the dynamics of the interior of the core could potentially lower the damping without substantially changing the nature of wave motion at the top of the stratified layer. We revisit this question in the next section on core angular momentum and LOD variations.

6 CHANGES IN CORE ANGULAR MOMENTUM

Fluctuations in the LOD on decadal timescale are usually attributed to changes in the angular momentum of the core (Bullard *et al.* 1950). A direct calculation of the core angular momentum can made using surface flows when the interior flow is assumed to be geostrophic (Jault *et al.* 1988). This approximation restricts fluid motion to be invariant in the direction of the rotation axis. As a result, core-surface flow can be extended into the interior. Many previous studies (e.g. Jault *et al.* 1988; Jackson *et al.* 1993) have used this approach to calculate changes in core angular momentum and found that the expected changes in LOD are consistent with observations. Only the $l = 1$ and 3 components of the zonal toroidal flow contribute to the core angular momentum, so we already have the core-flow models needed to reproduce the predictions of Jackson *et al.* (1993) and Gillet *et al.* (2015). Fig. 6(A) shows a comparison of the results of Jackson *et al.* (1993) with the observed LOD estimates (Gross 2001; Holme & de Viron 2013), after filtering the observations to remove fluctuations with periods of a year or less. The results of Gillet *et al.* (2015) are compared with the LOD observations in Fig. 6(B). Both of these flow models yield remarkable agreement with the observations, adding strength to the argument for geostrophic flow in the interior.

Stable stratification alters the nature of flow in the core (see Fig. 2), so it is reasonable to ask whether the observed fluctuations in LOD can be explained with MAC waves. As a first step toward answering this question we compute the angular moment associated with each wave and sum over the linear combination of modes that are fit to $\mathbf{v}_\phi$ at the core surface. The polar angular momentum is given by

$$L_z = \int_{V_l} \rho \mathbf{v}_\phi \, r \sin\theta \, \mathrm{d}V \tag{21}$$

where the volume of the stratified layer, V_l, accounts for only about 18 per cent of the moment of inertia of the entire core. The corresponding change in LOD is based on conservation of angular momentum

$$C_m \Delta\Omega_m + L_z = 0 \tag{22}$$

where $C_m = 7.12 \times 10^{37}$ kg m^2 is the polar moment of inertia of the mantle and $\Delta\Omega_m$ is the change in angular velocity of the mantle. The corresponding change in LOD, ΔT, is given by

$$\frac{\Delta T}{T} = -\frac{\Delta\Omega_m}{\Omega} \tag{23}$$

where T is the nominal period corresponding to Ω.

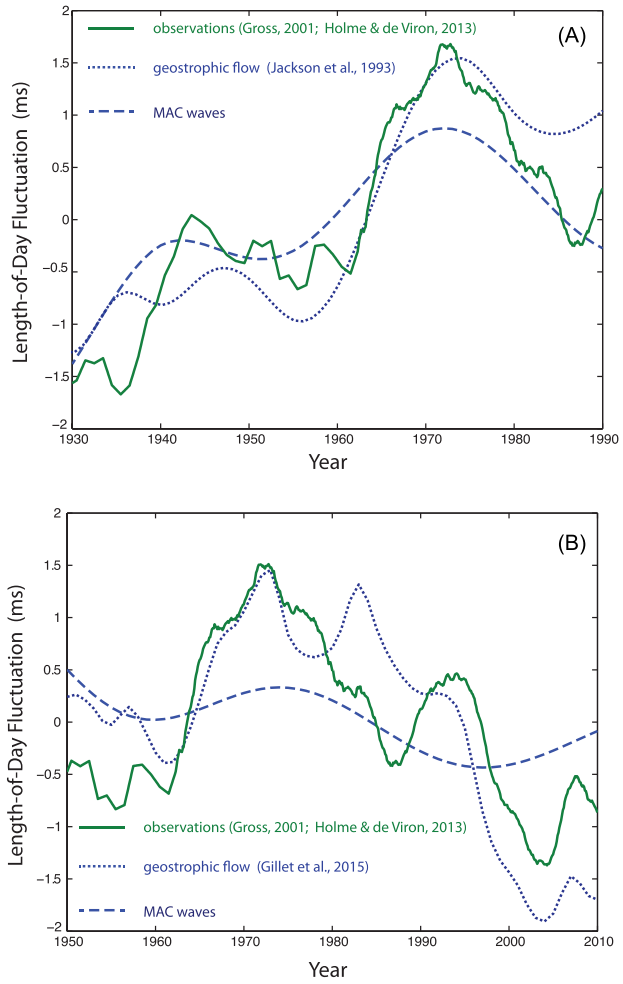

Figure 6. Length-of-day fluctuations compared with predictions using core-surface flows of (A) Jackson (1997) and (B) Gillet *et al.* (2015). Two types of predictions are presented. One is based on geostrophic flow (dotted line), while the other relies on the angular momentum carried by MAC waves in a stratified layer (dashed line). MAC waves must couple to motion below the stratified layer in order to account for the magnitude of the observed fluctuations.

Predictions for the MAC waves account for about half of the observed fluctuations between 1930 and 1990 (see Fig. 6A). Somewhat smaller fluctuations are predicted for MAC waves between 1950 and 2010 (see Fig. 6B), based on the flow model of Gillet *et al.* (2015). Neither of these results is entirely surprising because the stratified layer represents only a small fraction of the total moment of inertia of the core. In order to reconcile the amplitude of the observed fluctuations with MAC waves we need to account for motion in the interior of the core. Allowing for a deeper source of angular momentum could alter both the amplitude and phase of the LOD prediction.

Our calculations so far have assumed that the interior of the core is stationary (see Section 2.1). Wave motion is confined to the stratified layer, but electromagnetic stresses on the underlying fluid can drive motion through the entire core. The flow in the interior of the core is expected to be nearly geostrophic. Local stress drive a flow which takes the form of quasi-rigid fluid cylinders, but the response is not locally confined. Instead, nearby cylinders are coupled by the internal magnetic field (specifically by the cylindrical radial component B_s), allowing disturbances to propagate throughout the core as torsional waves. In other words, a full description of the interior response requires a treatment of torsional waves.

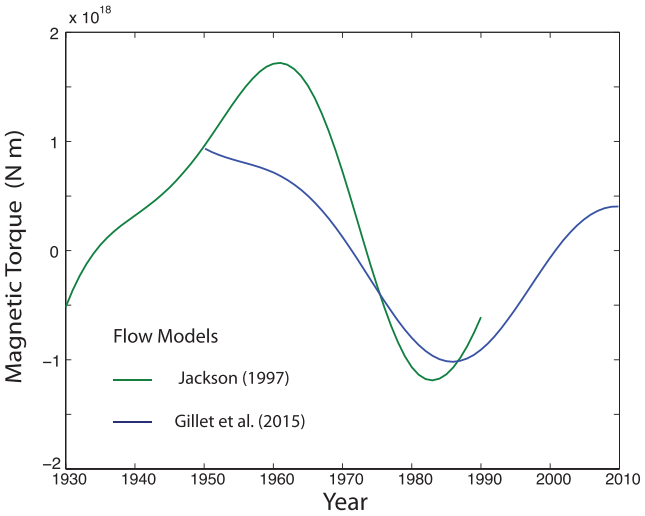

Figure 7. Electromagnetic torque at the base of the stratified layer due to MAC waves. Fluctuations in the torque are roughly $\pm 10^{18}$ N m^2 for both flow models. The corresponding changes in core angular momentum are sufficient to produce ± 5 ms fluctuations in length of day over periods of 60 yr.

A rough upper bound for the angular momentum change in the interior is computed from the total electromagnetic torque due to MAC waves. This calculation is liable to overestimate the actual torque because the underlying fluid is assumed to be static in our MAC-wave calculation. A large velocity discontinuity above a static interior ensures a large magnetic stress. Allowing the underlying fluid to adjust to these stresses would likely reduce the velocity discontinuity and lower the magnetic stresses. A general expression for the axial torque on the interior of the core is given by (Rochester 1962)

$$\Gamma_z = \frac{1}{\mu} \int_S \mathbf{B}_r \mathbf{b}_\phi \, r \sin\theta \, \mathrm{d}S \tag{24}$$

where the integral is taken over the surface at the base of the stratified layer ($r = r_i$). The steady radial field is approximated by a constant rms value of $\mathbf{B}_r = 0.62$ mT and the magnetic perturbation $\mathbf{b}_\phi$ at the base of the layer is taken from the MAC-wave calculation (with $\mathbf{v}^- = 0$).

Fig. 7 shows the predicted torque on the interior for our two sets of MAC waves. In both cases the predicted fluctuations are on the order of $\pm 10^{18}$ N m. In fact, the amplitudes of the torque are surprisingly similar where the predictions overlap. This agreement may be partly fortuitous because the angular momentum fluctuations associated with the two sets of MAC waves are somewhat different in amplitude (see Fig. 6). On the other hand, the phases of the angular momentum fluctuations are similar. It is not unreasonably expect a similar agreement in the phases of the torques. However, the agreement in the amplitudes of the torques means that the waves inferred from COV-OBS produce larger magnetic perturbations for the available angular momentum in the flow. This outcome is reasonable because a thinner layer means larger gradients in $\mathbf{b}$, which produce larger electric currents. Thus, a larger torque (relative to the amplitude of the flow) for COV-OBS is expected. Small differences in the radial structure of the two sets of MAC waves could also

contribute to the amplitude of the torque. The key point is that both cases yield torques with fluctuations on the order of $\pm 10^{18}$ N m. These fluctuations are sufficient to produce LOD fluctuations on the order of ± 5 ms over periods of 60 yr. By comparison, the observed fluctuations in Fig. 6 are closer to ± 1.5 ms over recent times, so the computed torques are too large by about a factor of 3. Weaker torques are possible when the dynamics of the interior are taken into account, but the preceding results show that MAC waves are capable of producing large fluctuations in the LOD. A more definitive assessment requires a fully coupled model for MAC waves and interior flow.

A simple model of coupled motion can be realized when torsional waves are fast enough to redistribute angular momentum through the core on timescales of several decades. Recall that torsional waves are characterized by periods of 4–6 yr (Gillet *et al.* 2010), which means that the periods of MAC waves are about an order of magnitude longer. At sufficiently low frequency, the interior fluid is expected to respond as a rigid body (see Appendix B). This motion would entrain the inner core through electromagnetic coupling, but a strong gravitational torque on the inner core resists any rotation relative to the mantle (Buffett & Glatzmaier 2000). When the gravitational torque is substantially larger than the electromagnetic torque at the top of the core, the interior (i.e. outer and inner cores) should remain nearly stationary as MAC waves propagate through the stratified layer.

To quantitatively explore this suggestion we express the gravitational torque on the inner core in the form

$$\Gamma_z = \gamma(\phi_m - \phi_i) \tag{25}$$

where ϕ_m and ϕ_i are the angular orientation of the mantle and inner core, respectively, relative to their positions in gravitational equilibrium, and γ is the amplitude of the torque. (The corresponding gravitational torque on the mantle is equal in magnitude but opposite in direction.) We take $\phi_m = 0$ on account of the large moment of inertia of the mantle and relate ϕ_i to rigid rotations of the interior of the core under the assumption that fast torsional waves redistribute angular momentum on timescales of several decades. Numerical calculations with the extended model show that the interior of the core becomes nearly stationary once γ reaches a value of 10^{21} N m. This value is about a factor of 5 larger than recent estimates (Davies *et al.* 2014), but our experiment illustrates one way in which waves above a static interior could be realized. In fact, the MAC waves in the coupled model that are nearly identical to those described earlier for an isolated stratified layer. We obtain good fits to core-surface flow and reproduce the observed the fluctuations in the dipole field. We also find that the amplitude of the gravitational torque on the mantle is sufficient to produce ± 5 ms fluctuations in LOD, consistent with our previous estimate based on MAC waves in an isolated stratified layer.

One way to improve our prediction is to reduce the strength of the gravitational torque. Setting $\gamma = 10^{20}$ N m brings the LOD fluctuations into better agreements with observations. We find a modest (20 per cent) increase in the misfit to the core-surface flow of Jackson *et al.* (2000), but the amplitude of the predicted dipole fluctuation is too small by a factor of 2. Thus, the simple coupled model cannot account for all of the observed phenomena. However, there are a number of ways to refine this simple model. Allowing the inner-core shape to viscously adjust adds another degree of freedom to the problem. Further flexibility is gained by removing the restriction of rigid-body motion in the interior. We may also need to consider a more general distribution of radial magnetic field in the stratified layer. Whether any of these generalizations are sufficient to reconcile all of the observations is presently unclear. However, our initial attempt at the coupled problem demonstrates that MAC waves can transfer enough angular momentum to the mantle to account for the observed fluctuations in LOD.

7 CONCLUSIONS

Axisymmetric MAC waves in a stratified layer at the top of the core offer a simple interpretation for several observed phenomena in the core. A linear combination of four to eight MAC waves gives a good description of time-dependent zonal flow at the top of the core (Jackson 1997; Gillet *et al.* 2015). The same set of waves can also account for observed fluctuations in the dipole field (Yokoyama & Yukutake 1991). Both of these predictions require a stratified layer with a thickness of roughly 130–140 km and a peak buoyancy frequency of $N_{\max} = 0.74\,\Omega$–$0.84\,\Omega$. MAC waves may also contribute to fluctuations in LOD, although the direct contribution from the waves explains only half (or less) of the observed amplitude. Allowing for electromagnetic coupling to the interior of the core, together with gravitational coupling to the mantle, can substantially increase the predicted fluctuations. In one idealized example, the predicted fluctuations in LOD are too large. Thus, generalizations of the coupled model may be needed to simultaneously account for time-dependent fluctuations in core-surface flow, dipole intensity and LOD.

Damping of the waves is recovered from fits to the core-surface flows. The level of damping is controlled primarily by the thickness of the layer, although the value of electrical conductivity in the core is also an important factor. Conventional values for σ (say $\sigma = 5 \times 10^5$ S m^{-1}) require thicker layers to match the core-surface flow, whereas higher σ permit thinner layers. We favour a thinner layer and a higher conductivity because the layer thickness also affects the amplitude of the dipole fluctuation. We obtain good agreement with the observed dipole fluctuation when $H \approx 140$ km and $\sigma = 10^6$ S m^{-1}. Adopting a lower σ, and consequently a thicker layer to match the core-surface flow, misfits the dipole fluctuation for a fixed value of $B_r = 0.62$ mT. Adopting a larger value for B_r could compensate for a thicker H when a lower value is chosen for σ (see Appendix A).

Excitation of MAC waves occurs when buoyant parcels in the convecting part of the core impinge on the base of the stratified layer. Transmission of radial motion into the stratified layer is expected to excite waves. Focusing of upwelling into the equatorial region could account for the preferential excitation of symmetric waves. While these waves do not discriminate between thermal and compositional stratification in the core, the thickness and strength of stratification are broadly consistent with a thermal origin (Gubbins *et al.* 1982). Thermal stratification is expected when the core heat flow, Q, is below a hypothetical heat flow, Q_a, conducted through a well-mixed region at the top of the core (often called the adiabatic heat flow). A simple model for thermal stratification predicts $H \approx 140$ km when $Q/Q_a \approx 0.87$ (Lister & Buffett 1998). An adiabatic heat flow of 15 TW (Pozzo *et al.* 2012) would correspond to $Q = 13.1$ TW. The predicted buoyancy frequency is $N_{\max} = 1.5\,\Omega$, which differs only by a factor of two from the values recovered from the MAC waves. Compositional stratification tends to yield much larger buoyancy frequencies (Buffett & Seagle 2011; Gubbins & Davies 2013), although a variety of processes, such as double-diffusive convection or wave-driven mixing, could reduce the strength of core stratification. Thus, a compositional origin cannot be ruled out.

ACKNOWLEDGEMENTS

This work is partially supported by grant EAR-1430526 to Bruce Buffett from the National Science Foundation and by grant NE/M012190/1 from National Environment Research Council. Richard Holme was also supported through attendance on the CIDER programme. We thank Nicolas Gillet for help in using the COV-OBS geomagnetic field model and two anonymous reviewers for helpful comments and suggestions that improved the paper.

REFERENCES

Amit, H. & Olson, P., 2004. Helical core flow from geomagnetic secular variation, *Phys. Earth planet. Inter.,* **147,** 1–25.

Braginsky, S.I., 1970. Torsional magnetohydrodynamic vibrations in the Earth's core and variations in the length of day, *Geomagn. Aeron.,* **10,** 1–8 (Engl. Transl.).

Braginsky, S.I., 1984. Short-period geomagnetic secular variation, *Geophys. astrophys. Fluid. Dyn.,* **30,** 1–78.

Braginsky, S.I., 1993. MAC-oscillations of the hidden ocean of the core, *J. Geomag. Geoelectr.,* **45,** 1517–1538.

Bloxham, J., 1990. On the consequences of strong stable stratification at the top of the Earth's outer core, *Geophys. Res. Lett.,* **17,** 2081–2084.

Buffett, B., 2014. Geomagnetic fluctuations reveal stable stratification at the top of the Earth's core, *Nature,* **507,** 484–487.

Buffett, B.A. & Glatzmaier, G.A., 2000. Gravitational braking of inner-core rotation in geodynamo simulations, *Geophys. Res. Lett.,* **27,** 3125–3128.

Buffett, B.A., Matthews, P.M. & Herring, T.A., 2002. Modeling of nutation and precession: effects of electromagnetic coupling, *J. geophys. Res.,* **107,** B42070, doi:10.1029/2000JB000056.

Buffett, B.A., Mound, J. & Jackson, A., 2009. Inversion of torsional oscillations for the structure and dynamics of Earth's core, *Geophys. J. Int.,* **177,** 878–890.

Buffett, B.A. & Seagle, C.T., 2011. Correction to Stratification of the top of the core due to chemical interactions with the mantle, *J. geophys. Res.,* **116,** B07405, doi:10.29/2011JB008376.

Bullard, E.C., Friedman, C., Gellman, H. & Nixon, J., 1950. The westward drift of the Earth's magnetic field, *Phil. Trans. R. Soc. Lond. A,* **A243,** 67–92.

Christensen, U.R., 2011. Geodynamo models: tools for understanding properties of Earth's magnetic field, *Phys. Earth planet. Inter.,* **187,** 157–169.

Christensen, U.R., Aubert, J. & Hulot, G., 2010. Conditions for Earth-like geodynamo models, *Earth planet. Sci. Lett.,* **296,** 487–496.

Davies, C.J., Stegman, D.R. & Dumberry, M., 2014. The strength of gravitational core-mantle coupling, *Geophys. Res. Lett.,* **41,** 3786–3792.

Eymin, C. & Hulot, G., 2005. On core surface flows inferred from satellite magnetic data, *Phys. Earth planet. Inter.,* **152,** 200–220.

Fox, L. & Parker, I.B., 1968. *Chebyshev Polynomials in Numerical Analysis,* Oxford University Press.

Gillet, N., Jault, D., Canet, E. & Fournier, A., 2010. Fast torsional waves and strong magnetic field within the Earth's core, *Nature,* **465,** 74–77.

Gillet, N., Jault, D., Finlay, C.C. & Olsen, N., 2013. Stochastic modeling of the Earth's magnetic field: inversion for covariances over the observatory era, *Geochem. Geophys. Geosyst.,* **14,** 766–786.

Gillet, N., Jault, D. & Finlay, C.C., 2015. Planetary gyre, time-dependent eddies, torsional waves, and equatorial jets at the Earth's core surface, *J. geophys. Res.,* **120,** 3991–4013.

Gross, R.S., 2001. A combined length-of-day series spanning 1832–1997: LUNAR 1997, *Phys. Earth planet. Inter.,* **123,** 65–76.

Gubbins, D., Thompson, C.J. & Whaler, K.A., 1982. Stable regions in the Earth's liquid core, *Geophys. J. R. astr. Soc.,* **68,** 241–251.

Gubbins, D. & Roberts, P.H., 1987. Magnetohydrodynamics of the Earth's Core, in *Geomagnetism,* Vol. 2, pp. 1–184, ed. Jacobs, J.A., Academic Press, London.

Gubbins, D. & Davies, C.J., 2013. The stratified layer at the core–mantle boundary caused by barodiffusion of oxygen, sulphur and silicon, *Phys. Earth planet. Inter.,* **215,** 21–28.

Hide, R., 1966. Free hydromagnetic oscillations of the Earth's core and the theory of geomagnetic secular variation, *Phil. Trans. R. Soc. Lond., A,* **259,** 615–647.

Holme, R., 2015. Large-scale flow in the core, in *Treatise on Geophysics,* 2nd edn, Vol. 8, pp. 91–113, Elsevier, Amsterdam.

Holme, R. & de Viron, O., 2005. Geomagnetic jerks and a high-resolution length-of-day profile for core studies, *Geophys. J. Int.,* **160,** 435–439.

Holme, R. & de Viron, O., 2013. Characterization and implications of intradecadal variations in length of day, *Nature,* **499,** 202–204.

Jackson, A., 1997. Time-dependency of tangentially geostrophic core surface motions, *Phys. Earth planet. Inter.,* **103,** 293–311.

Jackson, A., Bloxham, J. & Gubbins, D., 1993. Time-dependent flow at the core surface and conservation of angular momentum in the coupled core-mantle system, in *Dynamics of Earth's Deep Interior and Earth's Rotation,* Vol. 72, pp. 97–107, American Geophysical Union Monograph.

Jackson, A., Jonkers, A.R.T. & Walker, M.R., 2000. Four centuries of geomagnetic secular variation from historical records, *Phil. Trans. R. Soc. Lond., A,* **358,** 957–990.

Jault, D., Gire, C. & LeMouël, J.-L., 1988. Westward drift, core motions and exchanges of angular momentum between core and mantle, *Nature,* **333,** 353–356.

Jault, D. & Finlay, C.C., 2015. Waves in the core and mechanical core-mantle interactions, in *Treatise on Geophysics,* 2nd edn, Vol. 8, pp. 225–244, Elsevier, Amsterdam.

Jones, C.A., 2011. Planetary magnetic fields and fluid dynamos, *Annu. Rev. Fluid Mech.,* **43,** 583–614.

Koot, L., Dumberry, M., Rivoldini, A., De Viron, O. & Dehant, V., 2010. Constraints on the coupling at the core-mantle and inner-core boundaries inferred from nutation observations, *Geophys. J. Int.,* **182,** 1279–1294.

Kuang, W. & Bloxham, J., 1999. Numerical modeling of magnetohydrodynamic convection in a rapidly rotating spherical shell: weak and strong field dynamo action, *J. Comput. Phys.,* **153,** 51–81.

Lehoucq, R.B. & Sorensen, D.C., 1996. Deflation techniques for an implicitly restarted Arnoldi iteration, *SIAM J. Matrix Anal. Appl.*, **17,** 789–821.

Lister, J.R. & Buffett, B.A., 1998. Stratification of the outer core at the core–mantle boundary, *Phys. Earth planet. Inter.,* **105,** 5–19.

Matsui, H., King, E. & Buffett, B., 2014. Multiscale convection in a geodynamo simulation with uniform heat flux along the outer boundary, *Geochem. Geophys. Geosyst.,* **15,** 3212–3225.

Pais, M.A. & Jault, D., 2008. Length of day decade variations, torsional oscillations and inner core super-rotation: evidence from recovered surface zonal flows, *Phys. Earth planet. Inter.,* **118,** 291–316.

Pozzo, M., Davies, C., Gubbins, D. & Alfe, D., 2012. Thermal and electrical conductivity of iron at Earth's core conditions, *Nature*, **485,** 355–358.

Rochester, M.G., 1962. Geomagnetic core-mantle coupling, *J. geophys. Res.,* **67,** 4833–4836.

Teed, R.J., Jones, C.A. & Tobias, S.M., 2014. The dynamics and excitation of torsional waves in geodynamo simulations, *Geophys. J. Int.,* **196,** 724–735.

Yokoyama, Y. & Yukutake, T., 1991. Sixty year variation in a time series of the geomagnetic Gauss coefficients between 1910 and 1983, *J. Geomag. Geoelectr.,* **43,** 563–584.

Zatman, S. & Bloxham, J., 1997. Torsional oscillations and the magnetic field within the Earth's core, *Nature,* **388,** 760–763.

APPENDIX A: DEPARTURE FROM TANGENTIAL GEOSTROPHY

Strict adherence to tangential geostrophy in a stably stratified layer ensures zonal flows, $\mathbf{v}_\phi$, that are purely azimuthal (Bloxham 1990). Introducing the effects of a radial magnetic field causes departures from tangential geostrophy, which are expressed as a small meridional flow, $\mathbf{v}_\theta$. The Coriolis force associated $\mathbf{v}_\theta$ is principally

balanced by Lorentz forces at low frequencies because the inertial effects are small. When radial gradients in $\mathbf{b}$ are large compared with horizontal gradients, the relevant force balance can be approximated by

$$f\mathbf{v}_\theta = \frac{\mathbf{B}_r}{\rho\mu}\,\partial_r \mathbf{b}_\phi \tag{A1}$$

where $f = 2\,\Omega\cos\theta$ is the Coriolis parameter. The magnetic perturbation, $\mathbf{b}_\phi$, is related to the azimuthal flow by

$$\partial_t \mathbf{b}_\phi = \mathbf{B}_r\,\partial_r \mathbf{v}_\phi + \eta\,\partial_r^2 \mathbf{b}_\phi \tag{A2}$$

where only the radial derivatives are retained in the diffusive term because the layer is thin. Approximating the diffusive term by

$$\eta\partial_r^2 \mathbf{b}_\phi \;\approx\; -\eta\frac{\pi^2}{H^2}\mathbf{b}_\phi \tag{A3}$$

and adopting a time dependence of $e^{i\omega t}$ yields

$$\left(i\omega + \eta\frac{\pi^2}{H^2}\right)\mathbf{b}_\phi = \mathbf{B}_r\,\partial_r \mathbf{v}_\phi \tag{A4}$$

or

$$i\omega\left(1 - i\frac{\pi^2}{2}\frac{\delta^2}{H^2}\right)\mathbf{b}_\phi = \mathbf{B}_r\,\partial_r \mathbf{v}_\phi \tag{A5}$$

on introducing the skin depth, δ, from (12). Thus, diffusive effects are small when the skin depth is small compared with the thickness of the layer.

Using the diffusion-free solution for $\mathbf{b}_\phi$ in the force balance (A1) gives

$$f\mathbf{v}_\theta = \frac{V_a^2}{i\omega}\,\partial_r^2 \mathbf{v}_\phi \tag{A6}$$

where $V_a = B_r/\sqrt{\rho\mu}$ is the Alfvén velocity associated with B_r. Finally, we quantify the magnitude of $\mathbf{v}_\theta$ by letting H/π characterize the lengthscale for radial variations in $\mathbf{v}_\phi$. The resulting relationship

$$f\mathbf{v}_\theta \approx i\frac{V_a^2\pi^2}{H^2\omega}\,\mathbf{v}_\phi \tag{A7}$$

shows that departures from tangential geostrophy depend on the strength of the radial magnetic field and the thickness of the stratified. Thinner layers are responsible for larger meridional flow, but also cause greater damping of the waves. To account for the observed dipole fluctuations we favour thinner layers and higher values for electrical conductivity, although thicker layers are also viable if the strength of the radial magnetic field is increased.

APPENDIX B: FORCED TORSIONAL OSCILLATIONS

MAC waves produce electromagnetic stresses on the underlying fluid. The motion of the interior is expect to take the form of torsional waves, although the frequency of this motion is an order of magnitude lower than the natural frequency of torsional waves. It is customary to describe torsional waves in terms of the angular velocity, $\zeta(s)$, of fluid cylinders as a function of cylindrical radius s. The governing equation for $\zeta(s)$ is essentially a statement of conservation of angular momentum for the fluid cylinders. When the time dependence of $\zeta(s)$ is specified by $e^{i\omega t}$, the governing equation can be written as (Braginsky 1970)

$$-\omega^2\, m(s)\zeta(s) = \frac{\mathrm{d}}{\mathrm{d}s}\left(\tau(s)\frac{\mathrm{d}\zeta}{\mathrm{d}s}\right) + i\omega f(s) \tag{B1}$$

where $m(s)$ is the moment density of the cylinder, $\tau(s)$ is the magnetic tension due to the average value of B_s^2 over the cylinders and $f(s)$ is the torque on the ends of the cylinders.

We are interested in the case where the motion is forced by f at frequencies ω much lower than the natural frequency, ω_0, of the torsional waves. In this case, the inertial term on the left-hand side of (B1) is nominally $(\omega/\omega_0)^2$ smaller than the leading order terms in (B1). Consequently, we approximate the forced motion using

$$\frac{\mathrm{d}}{\mathrm{d}s}\left(\tau(s)\frac{\mathrm{d}\zeta}{\mathrm{d}s}\right) + i\omega f(s) = 0 \tag{B2}$$

where $f(s)$ can include the influence of stresses from MAC waves at the base of the stratified layer ($r = r_i$), as well as stresses on the inner-core boundary. We confine our attention to stresses due to MAC waves and express $f(s)$ in the form

$$f(s) = 4\pi s^2\left(\frac{r_i}{z_f}\right)\left(\frac{B_r b_\phi}{\mu}\right) \tag{B3}$$

where $z_f = \sqrt{r_i^2 - s^2}$ is the axial position of the interface between the interior and the stratified layer. The electromagnetic torque on fluid cylinders inside radius $s = s'$ is

$$\Gamma_z(s') = \int_0^{s'} f(s)\,\mathrm{d}s \tag{B4}$$

so the total electromagnetic torque on the interior of the core is $\Gamma_z = \Gamma_z(r_i)$.

Departures from constant angular velocity (rigid rotation) are quantified by $d\zeta/ds$. Integrating (B2) over s and noting that $\tau(0) = 0$ yields

$$\frac{\mathrm{d}\zeta}{\mathrm{d}s} = -i\omega\frac{\Gamma(s)}{\tau(s)} \tag{B5}$$

It follows that departures from constant angular velocity are small when the frequency, ω, is small or the magnetic tension, τ, is large. To put this estimate for $d\zeta/ds$ into a more intuitive context, we evaluate the average angular velocity of the interior using angular momentum conservation

$$i\omega C_f(r_i)\bar{\zeta} = \Gamma(r_i) \tag{B6}$$

where

$$C_f(r_i) = \int_0^{r_i} m(s)\,\mathrm{d}s \tag{B7}$$

is the moment of inertia of the fluid interior (roughly 82 per cent of the entire moment of inertia of the core). Thus, a characteristic lengthscale, L, for the gradient in $\zeta(s)$ is

$$L^{-1} \equiv \frac{1}{\bar{\zeta}}\frac{\mathrm{d}\zeta}{\mathrm{d}s} = \frac{\omega^2 C_f(r_i)\Gamma_z(s)}{\tau(s)\Gamma_z(r_i)} \tag{B8}$$

A representative value for L exceeds the radius of the core when we take $B_s \approx 0.3$ mT and let $s \approx 0.5 r_i$. This means that a rigid-body rotation is a reasonable first approximation for the response of the interior when the internal magnetic field is strong enough to permit fast torsional waves.